

See discussions, stats, and author profiles for this publication at: <https://www.researchgate.net/publication/24415748>

The electromagnetic response of human skin in the millimetre and submillimetre wave range

Article in *Physics in Medicine and Biology* · July 2009

DOI: 10.1088/0031-9155/54/11/005 · Source: PubMed

CITATIONS

45

READS

288

7 authors, including:



Yuri D Feldman

Hebrew University of Jerusalem

217 PUBLICATIONS 3,970 CITATIONS

SEE PROFILE



Alexander Puzenko

Hebrew University of Jerusalem

57 PUBLICATIONS 913 CITATIONS

SEE PROFILE



Paul Ben Ishai

Ariel University

74 PUBLICATIONS 819 CITATIONS

SEE PROFILE



Andreas Caduff

Biovotion

55 PUBLICATIONS 1,047 CITATIONS

SEE PROFILE

Some of the authors of this publication are also working on these related projects:



Microwave near-field probe [View project](#)



Dielectric Response of Cytoplasmic Water and Its Connection to the Vitality of Human Red Blood Cells [View project](#)

The electromagnetic response of human skin in the millimetre and submillimetre wave range

This article has been downloaded from IOPscience. Please scroll down to see the full text article.

2009 Phys. Med. Biol. 54 3341

(<http://iopscience.iop.org/0031-9155/54/11/005>)

[The Table of Contents](#) and [more related content](#) is available

Download details:

IP Address: 132.64.1.37

The article was downloaded on 10/05/2009 at 17:46

Please note that [terms and conditions apply](#).

The electromagnetic response of human skin in the millimetre and submillimetre wave range

Yuri Feldman^{1,3}, Alexander Puzenko¹, Paul Ben Ishai¹,
Andreas Caduff^{1,4}, Issak Davidovich¹, Fadi Sakran¹ and
Aharon J Agranat^{1,2}

¹ Department of Applied Physics, The Hebrew University of Jerusalem, Givat Ram, 91904, Jerusalem, Israel

² The Interdisciplinary Center for Neural Computation, The Hebrew University of Jerusalem, Givat Ram, 91904, Jerusalem, Israel

E-mail: yurif@vms.huji.ac.il

Received 3 December 2008, in final form 23 February 2009

Published 8 May 2009

Online at stacks.iop.org/PMB/54/3341

Abstract

Recent studies of the minute morphology of the skin by optical coherence tomography revealed that the sweat ducts in human skin are helically shaped tubes, filled with a conductive aqueous solution. This, together with the fact that the dielectric permittivity of the dermis is higher than that of the epidermis, brings forward the supposition that as electromagnetic entities, the sweat ducts could be regarded as low Q helical antennas. The implications of this statement were further investigated by electromagnetic simulation and experiment of the *in vivo* reflectivity of the skin of subjects under varying physiological conditions (Feldman *et al* 2008 Phys. Rev. Lett. **100** 128102). The simulation and experimental results are in a good agreement and both demonstrate that sweat ducts in the skin could indeed behave as low Q antennas. Thus, the skin spectral response in the sub-Terahertz region is governed by the level of activity of the perspiration system and shows the minimum of reflectivity at some frequencies in the frequency band of 75–110 GHz. It is also correlated to physiological stress as manifested by the pulse rate and the systolic blood pressure. As such, it has the potential to become the underlying principle for remote sensing of the physiological parameters and the mental state of the examined subject.

1. Introduction

The human skin is the largest organ of the integumentary system which constitutes the interface between the body and its surrounding environment (Graham-Brown and Burns

³ Author to whom any correspondence should be addressed.

⁴ Present address: Solianis Monitoring, Leutschenbachstrasse 46, Zurich 8050, Switzerland.

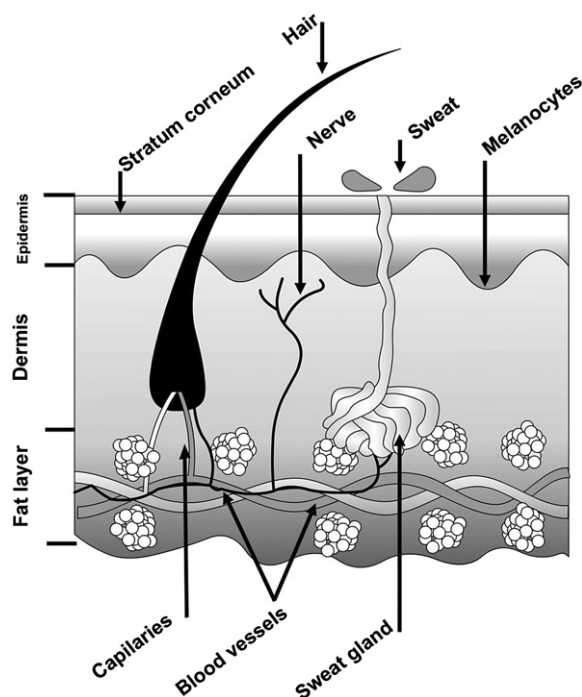


Figure 1. Schematic presentation of the skin morphology.

2002). The morphology of the skin constitutes a complex multilayered structure in which several subsystems are interlaced, including blood vessels and capillaries, the sebaceous glands, various extensions of the nervous system, hair and their follicles (figure 1) (Jacobovic and Ackerman 1992).

In particular, the skin is the platform for the perspiration system. The latter consists of the sweat glands that are situated at the bottom of the dermis and are deployed throughout the skin. The primary function of the sweat glands is thermoregulation; they also participate in controlling the water content and ions balance. There are two types of sweat glands, ordinary eccrine sweat glands found over most of the body and large apocrine sweat glands of auxiliary, pubic and perianal regions (Jacobovic and Ackerman 1992). Each eccrine sweat gland consists of a secretory coil situated deep in the dermis, and a duct which conveys the secreted sweat to a pore on the stratum corneum, the outer layer of the skin. In response to innervation by the peripheral nervous system via the central nervous system, the sweat glands secrete the sweat liquid into the sweat ducts. The ducts carry the sweat to the pores where it is secreted to the skin surface and evaporates (Goldsmith 1999). Although the coil-like structure of the ducts was noticed a long time ago (Takagi and Tagawa 1957), in most anatomical textbooks, this morphology is not considered and the sweat ducts are usually shown as a straight tube (Jacobovic and Ackerman 1992, Goldsmith 1999). In fact, in the eccrine sweat glands, the end part of the duct that is embedded in the epidermis and leading to the pore is helical rather than straight. Consider figure 2 in which a detail of an image of the skin produced by optical coherent tomography is presented (Knüttel and Böehlau-Godau 2000, Knüttel *et al* 2004). The coil-like nature of the end part of the duct situated in the epidermis is clearly seen in this image.

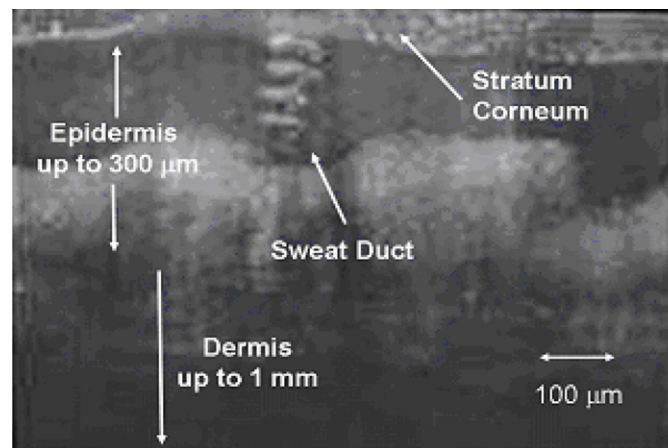


Figure 2. 3D optical coherence tomography image (reproduced with permission from ISIS GmbH) of a single sweat duct in the epidermis layer (Feldman *et al* 2008). (Reproduced with permission from Feldman *et al* (2008); Copyright 2008, American Physical Society.)

When considering the helical nature of the final portion of the duct and the difference in dielectric permittivities between the dermis and the epidermis (Gabriel *et al* 1996, Grimnes and Martinsen 2000), one can assume that the ducts could act as low Q helical antennas. A coil at the end of a typical sweat duct has, on average, four to six turns with diameters about $100\ \mu\text{m}$. The coil is embedded in the epidermis over a length of $300\ \mu\text{m}$. Taking all this into account, the coils at the end of the sweat ducts are expected to resonate at approximately 100–1000 GHz, namely at the extremely high frequency range (EHF) (Balanis 2005, Kraus 1950). Inherent to this supposition is the requirement that the duct possesses an electrical conductance mechanism that is effective at the EHF range. Even though the ducts are filled with conducting electrolytes, the mobility rates of the ions are slow ($\sim 10^{-7}\ \text{m s}^{-1}$) compared to the extremely high frequencies required to support resonance in the duct coil. A mechanism that qualifies for such a requirement is fast proton hopping through distributed H-bond networks along the duct surface. It is well established that these networks exist in biological structures (Sadeghi and Cheng 1999) and it was found that the characteristic time for such proton transport is about $10^{-13}\ \text{s}$ (Krasnoholovets *et al* 2003). Taking into consideration the potential drop caused by the difference in the pH value between the skin surface and the dermis (Guyton 1991), the proton hopping mechanism can account for the ac conductivity that is necessary for the sweat ducts to yield an electromagnetic response in the EHF range. As the sweat system activity is known to be correlated with the physiological and emotional state (Ogawa and Sugeno 1993), changes in these physiological and emotional stimuli should be expressed in the electromagnetic response of the skin. In our previous work (Feldman *et al* 2008), we demonstrated that this structure is indeed electromagnetically active and can act as an imperfect helical (i.e. non-metallic) antenna in the millimetre–submillimetre wave range. The experimental results were compared to a computational study of the propagation of an electromagnetic beam in an idealized section of the skin containing eight helical sweat ducts, which theoretically represent a skin area of approximately $5\ \text{mm}^2$. Here, we will present the experimental details and the main features of the model used for verification of our hypothesis.

2. A theoretical model of the human skin electromagnetic response

The human skin is a complex organ, and therefore some simplifications have to be introduced due to the obvious differences between biological tissue and a classic electromagnetic model (Grimnes and Martinsen 2000). In an electromagnetic model, all the sources (charges, currents, voltages or the modes of the wave electromagnetic field excitation) should be well defined. In particular, as we mentioned above, the high frequency current in ducts may be due to the proton hopping. Ionic flow would produce currents at frequencies too low to be considered in our simulation model and are therefore ignored. The difference of the electric potential may be due to the pH gradient or because of the gradient in a membrane potential. An idealized section of the skin has to be designed and the materials in subdomains are clearly categorized by their electrical properties.

In general, electromagnetic waves in an inhomogeneous media can be described in terms of a 4×4 polarization scattering matrix of the monochromatic plane waves by which two orthogonal polarizations are taken into account in the scattering problem (Pojar 1998). In the particular case of the same polarization of incidence and scattering waves (i.e. the same polarization of the source/end receiver of the electromagnetic radiation), the problem can be reduced to the 2×2 scattering matrix, $\hat{S}(\omega)$, where $\omega = 2\pi f$ and f is the frequency (Pojar 1998):

$$\hat{S}(\omega) = \begin{pmatrix} S_{11}(\omega) & S_{12}(\omega) \\ S_{21}(\omega) & S_{22}(\omega) \end{pmatrix}. \quad (1)$$

Here, the element $S_{11}(\omega)$ is the reflection coefficient equal to the ratio of the complex magnitudes of the reflected plane wave, $U_{\text{ref}}(\omega)$, to incidence plane waves, $U_{\text{in}}(\omega)$:

$$S_{11}(\omega) = \frac{U_{\text{ref}}(\omega)}{U_{\text{in}}(\omega)}. \quad (2)$$

Similarly, the element $S_{21}(\omega)$ is the propagating coefficient equal to the ratio of the complex magnitudes of propagated, $U_{\text{prop}}(\omega)$, to incidence, $U_{\text{in}}(\omega)$, plane waves:

$$S_{21}(\omega) = \frac{U_{\text{prop}}(\omega)}{U_{\text{in}}(\omega)}. \quad (3)$$

Thus, the phenomena of radiation and absorption by human skin in the EHF frequency band can be quantified within the framework of an appropriate electromagnetic model in terms of the scattering matrix. Such a framework will investigate a number of possible physical phenomena, for instance the reflection of electromagnetic waves from a multilayered skin model; the nature of the current in the sweat ducts as a source of electromagnetic radiation and the interaction of the surrounding electromagnetic field within the layered dielectric medium with the ducts of different resistance and inductance.

2.1. Human skin description and electromagnetic skin model configuration

The skin organ is the primary interface, utilizing numerous functions and interactions, between us and our environment. The complexity of the multilayered skin morphology provides a broad range of features in sensory and control functions that utilize a number of physical phenomena. It is richly innervated, with a variety of sensory nerve endings which respond to a broad range of excitations, such as pressure, vibration, heat, cold, itching or pain, and by motor nerve endings which control blood flow, sweat secretion or piloerection (Jacobovic and Ackerman 1992).

The stratum corneum (SC) is the outermost layer of the skin. It is composed mainly of dead cells that lack nuclei. Cells of the SC contain keratin that helps keep the skin hydrated by preventing water evaporation. The SC covers the epidermis, a hard and tough layer. It is our main protection against ultraviolet radiation and holds melanocytes, which produce the pigment melanin and give the skin its characteristic colour. When covering sensitive parts of the body, such as the eyelids, the epidermis is only 0.05 mm thick, but on heavily used parts of the body, like the palms of the hands or the soles of the feet, this layer can be up to 1.5 mm thick. The next layer is the dermis, which also can vary in thickness depending on what part of the body it is covering. On the back, it can be up to 3.0 mm thick and on the eyelids again only 0.3 mm thick (Nouveau-Richard *et al* 2004, Neerken *et al* 2004, Sandby-Moller *et al* 2003). At locations on the body with high densities of eccrine sweat glands, the thicknesses of the epidermis and dermis are closer to those of the eyelid, rather than those of the back. Hence, in our simulations, we set 0.1 mm for the epidermis and 1 mm for the dermis (Waller and Maibach 2005). The layered skin structure allows us to design an appropriate multilayer model with specific structural and electrical properties of each subdomains. For simplicity, each skin layer can be defined as uniform with well-defined sharp boundaries and its own electrical and structural properties. The first step in building the skin model for electromagnetic simulation is to create components such as SC, epidermis, and dermis and sweat ducts with proper structural and materials definitions.

In the 3D electromagnetic simulation software, several different material properties are considered to allow realistic modelling of practical simulation problems. The basic material can be defined by its dielectric permittivity and its conductivity. It is known that water has a strong dielectric dispersion in the microwave frequency range (Ellison *et al* 1996). At the same time, the multilayer skin is a heterogeneous material and contains other non-dispersive components. Therefore, the skin model considers two types of materials, water and all other components (lipids, proteins, fat, etc) that are considered to be non-dispersive at the frequencies of interest (Pethig 1987, Smith and Foster 1985). For simplicity, intercellular displacement currents are ignored.

There are a number of mixture formulae suited to calculate the bulk dielectric response of binary systems. If domain boundary effects are ignored, then the correct formula will lie between the extreme cases of separate layers (extreme anisotropy) to a spatially homogenous distribution of spheres in a dielectric background (the Maxwell–Wagner model). However, when taking the parameters of water and the dry skin components in our frequency window, we found that the variation between the two extreme cases to be small. In terms of the real component of the complex permittivity of the mixture, it is less than 0.1. Consequently, the permittivity of the mixtures can be derived by the Maxwell–Wagner equation given by Pethig (1979), Takashima (1989):

$$\varepsilon_{\text{mix}} = \varepsilon^{\text{bm}} \frac{(2\varepsilon^{\text{bm}} + \varepsilon^w) - 2\phi(\varepsilon^{\text{bm}} - \varepsilon^w)}{(2\varepsilon^{\text{bm}} + \varepsilon^w) + \phi(\varepsilon^{\text{bm}} - \varepsilon^w)}, \quad (4)$$

where ε^{bm} is the permittivity of the dry biological structural components, ε^w is a permittivity of water and ϕ is the volume fraction of the water component. The maximum permittivity of the dry biological structure according to the literature is about 2.2 (Pethig 1987). The water content of the different skin layers was measured using combined confocal Raman micro spectroscopy and confocal laser microscopy measurements. It was found that in the SC, the water content is 10–15%; in the epidermis, 45–55% and in the dermis, 70–80% (Caspers *et al* 2000). However, it is known that water in biological materials exists in two states: bulk and hydrated. Moreover, it is also known that the hydration rate in biological tissues is quite

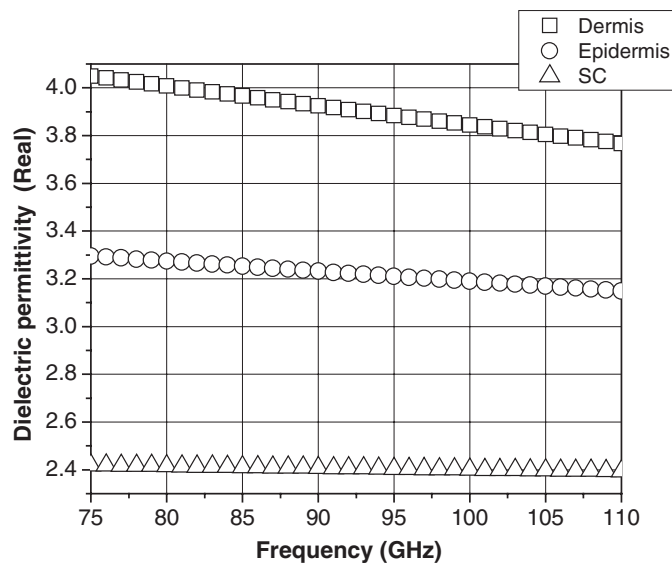


Figure 3. The dielectric permittivity of different skin layers in the frequency range from 75 GHz to 110 GHz. For clarity, only the real component of the dielectric permittivity is shown.

high and can even reach 80% (Wang *et al* 1999). Consequently, in the considered frequency range, the contribution of the bulk water to the complex dielectric permittivity is significantly smaller and its volume fraction in formula (4) must be decreased accordingly. Note that the dielectric response of bound water is out of the frequency band of interest (<1 GHz).

It is well known that the complex permittivity $\varepsilon^w(\omega)$ of bulk water in the EHF frequency band can be described by the Cole–Cole relationship (Kaatze 1989, Peyman *et al* 2007):

$$\varepsilon^w(\omega) = \varepsilon_\infty + \frac{\varepsilon_s - \varepsilon_\infty}{1 + (i\omega\tau_0)^{1-\alpha}}, \quad (5)$$

where ε_∞ is the high frequency permittivity, ε_s is the static permittivity, τ_0 is the relaxation time of the process and α is the broadening parameter. Using relationship (5) and the Maxwell–Wagner equation for mixtures, the effective layer permittivity was calculated taking into account the following volume fraction of bulk water in the corresponding layers: SC 4%; epidermis 18% and dermis 28%. The real component of the dielectric permittivity of each skin layer as a function of frequency is presented in figure 3.

The results showed that in the 75–110 GHz frequency band, the skin permittivity has insignificant variations. The electrical properties of the SC are almost constant in this frequency band. The epidermis has small variations, and the dermis, due to the biggest water content, has slightly higher frequency dependence in this frequency range compared to the other layers.

The conductivity of each layer was determined by a simple consideration of blood content in each layer. The dc conductivity of the dermis, epidermis and SC is about 0.2 S m^{-1} , 0.025 S m^{-1} , 10^{-5} S m^{-1} , respectively (Pethig 1987, Peters *et al* 2001). However, the effective conductivity of the dermis and epidermis is much greater. The conductivity of the blood at 100 GHz is about 60 S m^{-1} (Gabriel *et al* 1996); therefore, it is reasonable to assume that the high-frequency conductivity of the dermis is about 40 S m^{-1} . Furthermore, it is known

Table 1. Parameters of the basic 3D skin model—layers.

Layer	dc conductivity (S m ⁻¹)	ac conductivity at 100 GHz (S m ⁻¹)	Permittivity	Layer width (μm)
Dermis	0.1	30	3.9	1000
Epidermis	0.01	1	3.2	350
SC	10 ⁻⁵	10 ⁻⁵	2.4	30

that the epidermis contains a negligible amount of blood vessels with less water compared to the dermis. Therefore, the estimated conductivity of the epidermis at 100 GHz is about 1 S m⁻¹. The SC is composed of dry dead cellular material and its conductivity is consequently minimal. For convenience, it was decided that for the simulation skin model, the layer's conductivity in all frequencies (75–110 GHz) will be equal to the conductivity of the layer at 100 GHz. The parameters of the basic 3D skin model are presented in table 1.

2.2. Current mechanism

The ducts of the eccrine sweat glands have tubular structures similar to helices. Being filled with electrolytes (such as Na⁺ and Cl⁻ in water), they are the organic equivalent of inductance coils in electric circuits. Due to the fact that the duct is all the time full with aqueous electrolyte solution (sweat), it is reasonable to assume that a hydrogen-bonded network exists in the inner surface of the duct (Sadeghi and Cheng 1999). Taking into account that the proton average hopping time in a hydrogen-bonded network is about 10⁻¹³ s (Krasnoholovets *et al* 2003), it is reasonable to assume that in such a network, there is a high frequency proton transport. The supporting literature suggests that it is extremely fast (Cukierman 2000). Therefore, it could be that the proton current along the cells of the spiral sweat duct can be considered as instantaneous and the resonant frequency of the duct would be determined by the geometrical structure. However, for any meaningful electromagnetic response, an electro-motive force would be required. The pH value of the skin surface is 5.5 and the pH of the dermis is about 6.7 (Guyton 1991) leading to the gradient of the proton concentration along the duct given by Covington *et al* (1985):

$$[H^+] = 10^{-5.5} - 10^{-6.7} = 2.96 \times 10^{-6} \text{ mol l}^{-1}. \quad (6)$$

Macroscopically, the passage of the protons through the hydrogen-bonded network is diffusive in nature. The implication of (6) is that there exists in this diffusion a dominant drift toward the dermis. Thus, the average ac current would not be equal to zero. It is the combination of such an electrical gradient and the short proton lifetimes in the network that may produce the EHF current. The sweat ducts were modelled as conducting coils of two to four turns with diameters 60–80 μm and heights 300–350 μm (figure 4).

The stability of the hydrogen network inside the coil depends on the presence of hydration centres, for example Na⁺/K⁺ or Cl⁻ ions, in its vicinity. Hence the resultant level of proton conductivity is expected to exhibit a direct dependence on the sweat rate, itself a measure of physical effort (Inoue *et al* 1998). Therefore, the conductivity of the coil can be used as the parameter that quantifies the level of relaxation following intense physical activity or emotional excitation (Perini *et al* 1989), i.e. it is expected that the conductivity of the coil will follow the same time dependence as the decay of sweat flow in the ducts. Amongst the various component of the skin tissue, the level of sweating in the sweat duct plays a dominant

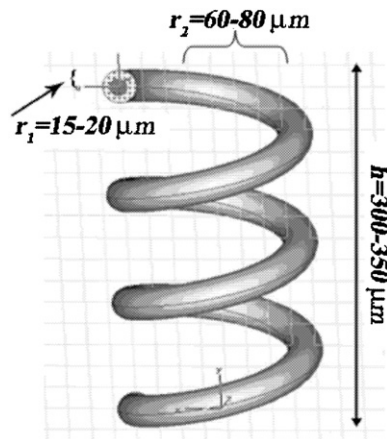


Figure 4. The idealized sweat duct used in the simulation software ‘CST Microwave Studio’ with the relevant dimensions. The sweat duct coil was modelled as a helical pipe filled with electrolyte. It is permanently full of sweat and so there exists a hydrogen bond network along the surface. (Reproduced with permission from Feldman *et al* (2008); Copyright 2008, American Physical Society.)

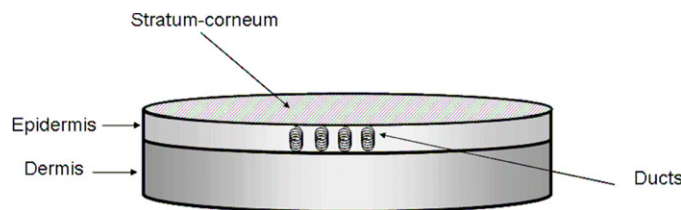


Figure 5. The model used for 3D electromagnetic simulations. The disk represents a portion of skin consisting of three separate layers and an array of eight sweat ducts. (Reproduced with permission from Feldman *et al* (2008); Copyright 2008, American Physical Society.)

Table 2. Parameters of the model sweat duct.

Duct total length	Duct height (μm)	Number of turns	Permittivity	Conductivity- σ (S m^{-1})
~ 1500	300–350	2–4	3.8–4	2500–10000

role setting the duct conductance (Shamsuddin and Togawa 1998). Hence, it is expected that the electromagnetic response of the coils at the tip of the ducts will be strongly affected by the level of activity of their respective glands. Table 2 shows the properties of one duct in the skin model. Different conductivity correlates to different proton concentration in the network, and therefore different current in the sweat duct.

Taking into consideration the three-layer skin model and the model of the sweat duct, we built the 3D model of the skin portion with eight embedded helical ducts into the epidermis layer (see figure 5).

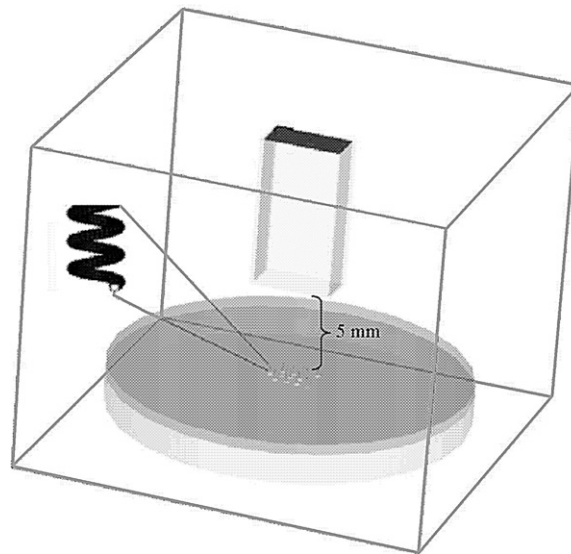


Figure 6. Skin model with eight active ducts radiated by a waveguide.

Based on our skin model, we designed the 3D electromagnetic simulation model that can support real experimental results.

2.3. The 3D electromagnetic simulation with the radiation of the 3D skin model by the outer radiation source

3D electromagnetic simulations utilize a 3D full-wave Finite Element method (FEM) to solve the electromagnetic equations (Maxwell) over a mesh of nodes covering a 3D model. The simulation package CST Microwave Studio was found to be the most appropriate software tool to solve the proposed problem.

A waveguide with aperture dimensions of 2.54×1.27 mm (WR10) and a length of 7 mm operating in the frequency band of 75–110 GHz (W band) is placed above the skin model (see figure 6). One of the two waveguide apertures is defined as a wave port, i.e. it generates an incident electromagnetic wave on the skin surface according to the simulation and frequency settings. The wave port also has functionality of absorbing the returning radiation, for the calculation of scattering matrix S -parameters. The opposite waveguide aperture is attached to the model container—a simple box filled with air. The faces of that container are defined as open radiation boundaries, i.e. the electromagnetic waves can pass this boundary with minimal reflections. The skin model (the object that is being measured) is set in the container, 3–5 mm from the waveguide aperture.

Using this configuration, it is possible to measure EM wave reflection from any object that is placed into the container. Note that the reflected EM signal in the wave port contains reflections from different elements of the model. It includes the reflection from the multilayers of the model media, reflections from the sample edges (diffraction effects), reflections from the waveguide aperture attached to the container, reflection from the system boundaries—container walls.

The reflection from the sample surface is considered as the useful signal and all of the other reflections are considered as noise, which needs to be filtered. The wave

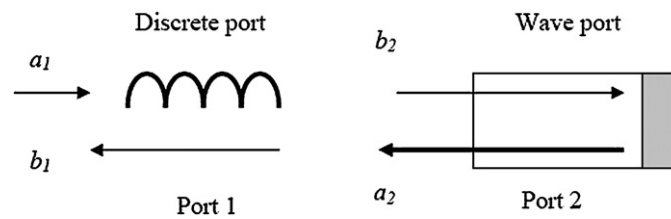


Figure 7. Schematic presentation of the two-port system.

diffraction by the sample edges is reduced by enlarging the skin model dimensions until the dimensions no longer influence the reflection from the skin model. The reflection from the waveguide aperture is reduced by smoothing the aperture edges. The reflection from the system boundary is reduced by enlarging the dimensions of the system, i.e. enlarging the container.

In order to model the sweat duct as an electromagnetically active unit, two types of excitation port were designed in the model and are schematically represented by figure 7. A discrete port is attached to each duct and simulates possible duct excitations by an independent ac current source inside the duct. The wave port is used to generate the incident waves and to measure the total radiation coming back from the model. In the active two-port regime the total radiation measured includes both reflected EM waves from the skin model and emitted EM waves from the ducts.

The first set of simulations was considered as a calibration where the best configuration (i.e. sizes of the skin model and container) for the specific model was obtained in order to reduce parasitic effects arising from the boundary conditions of the container. Wave ports in CST are defined as a special kind of boundary condition, enabling the stimulation as well as the absorption of energy. In this simulation, the ac conductivity of each duct was equal to $\sigma = 3500 \text{ (S m}^{-1}\text{)}$, a value of conductivity that is not far from the values for sweat ducts as reported in the literature (Cukierman 2000).

There are two steps in obtaining total radiation in the wave port. The first step is the reference simulation, in which the ducts are passive, i.e. they are not excited; another option to achieve passive behaviour of the ducts is to set the conductivity of the ducts to be very low ($500\text{--}1000 \text{ S m}^{-1}$). The second step is the simulation of all the ducts excited with their conductivity ranging from 3500 to 6000 S m^{-1} . The chosen values of the duct conductivity are not far from the real values for proton conductivity that can take place in the duct. The conductivity in a hydrogen-bonded network is proportional to the proton concentration in the network. It is well known that natural relaxation processes in the human body, such as the blood pressure after physical activity, relax exponentially (Perini *et al* 1989). Additionally, it was reported in the literature (Inoue *et al* 1998, Shamsuddin and Togawa 2000) that there is an exponential decrease in the sweat rate during relaxation. As inherent hydration centres, such as salts, would have more opportunity to disrupt H-bond networks as the sweat rate decreases, it is reasonable to assume that the ac conductivity in the sweat duct will be proportional to the exponential decreasing of the sweat rate. Therefore, the duct conductivity will have an exponential decrease of its conductivity. Based on this rationale, the total radiation in the wave port for different values of the duct conductivity is presented in figure 8.

When all the ducts in the skin model are excited, the simulation shows a clear dependence of the minimum of the reflection coefficient on the conductivity of the coil. In general, the conductivity depends on the flow of sweat in the duct (Perini *et al* 1989).

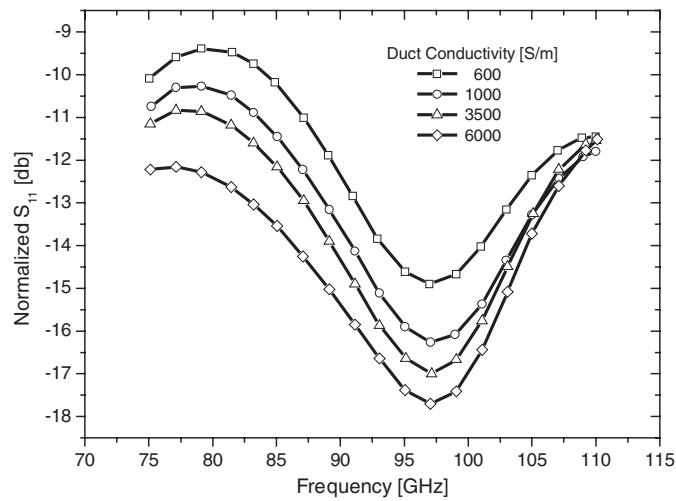


Figure 8. Simulation results of the skin model with eight ducts. The duct ac conductivity is varied exponentially.

3. Experimental observation

To test the validity of our predictions and simulations we conducted a series of *in vivo* measurements of the hand palm skin reflection coefficient for several subjects. The measurements were done using a vector network analyser (VNA HP 8510C) in the spectral range of 75–110 GHz (W Band) (Feldman *et al* 2008). The results of these measurements demonstrated that the electromagnetic response in this frequency band strongly changes after intense physical activity. It will be shown that these results cannot be interpreted on the basis of changes in the water content of the skin. However, the observed changes are strongly correlated with both the blood pressure and the heart pulse rate, and the significance of these findings and their applicability will be discussed.

3.1. Experimental details

In order to substantiate the existence of the electromagnetic response of human skin, *in vivo* measurements were provided in the frequency range 75–110 GHz using near field (NF) and distance measurement (DM) configurations. All the measurements were provided in the air-conditioned environment with the control temperature around 23 °C.

3.1.1. 'Near field' setup. A series of NF simultaneous measurements of the amplitude and phase reflected from the palm of the subjects were carried out through the frequency range between 75 GHz and 110 GHz. The NF setup is illustrated schematically in figure 9. The setup is based on the HP-8510C VNA for which an HP-83558A millimetre wave module and an HP-83623 sweep oscillator were used as the source. The VNA input/output WR-10 waveguide was operated in the fundamental mode (TE_{10}) and was connected to a pyramidal horn antenna covered with a 3 mm thick Teflon plate. The subject's palm was mounted on the Teflon plate.

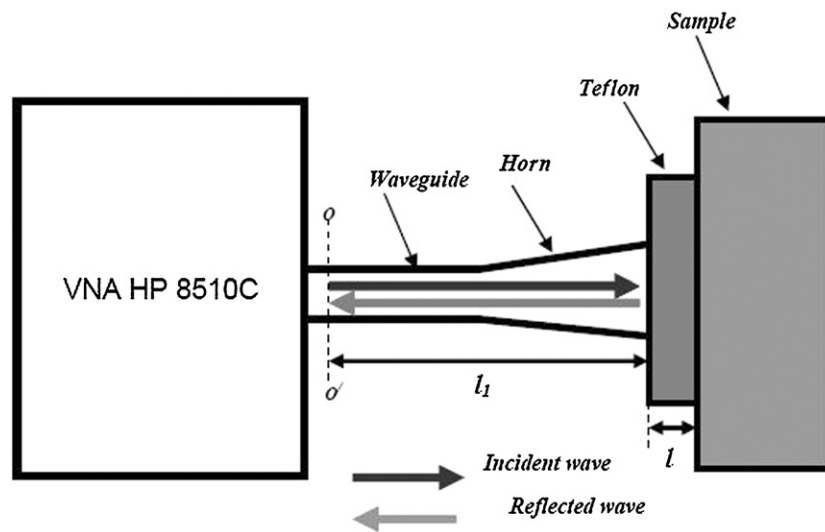


Figure 9. Schematic representation of the VNA matched to the waveguide with the horn antenna terminated by a Teflon plate with the sample under investigation. Here l_1 is the distance from the section OO' to the Teflon plate and l is the thickness of the Teflon plate.

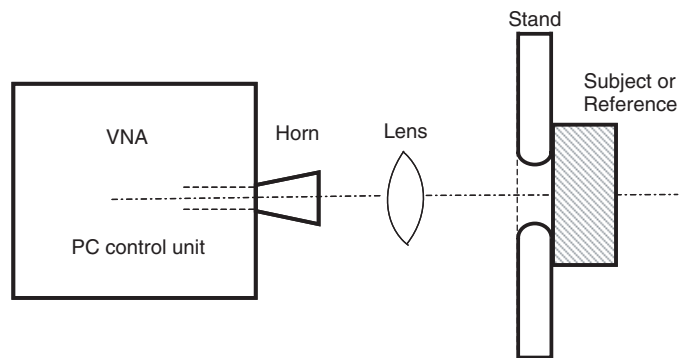


Figure 10. Schematic presentation of the measurement system in the 'Distance Measurement' configuration with the lens and hand palm stand.

The effects of multiple reflections in the setup and background noise that occur in free space measurements were cancelled out by applying a special calibration procedure to the setup (see the details in appendix A).

3.1.2. 'Distance measurement' setup. The second set of measurements in the frequency range of 75–110 GHz was done in a system that was configured for distance measurements, as shown in figure 10. The VNA was connected to a pyramidal horn antenna operating in the main mode (TE_{10}) through a WR-10 waveguide. The Teflon lens was located 42 mm from the horn and was used to decrease the diffraction effects and enhance the reflected power. A stand was designed in order to stabilize the palm during the measurements as well as to allow accurate positioning of the palm relative to the horn. It was made from Delerlin, a low-loss

polymer in the measurement frequency band, with the permittivity of ~ 3.5 . This relatively low dielectric permittivity reduces reflections from the stand surfaces. The stand has a circular hole with a diameter of 60 mm. In order to decrease the diffraction losses, the edge of the hole on the horn side was bevelled smooth with the curvature radius close to the thickness of the stand. The palm was placed over the hole, at a distance of 220 mm from the horn.

3.1.3. Subjects. Three female and eight male healthy volunteers ranging between 27 and 35 years of age participated in this study with the approval of the Ethical Committee of the Hebrew University of Jerusalem. They were informed about exposure duration, intensity and frequency relevant to human health and freely gave their consent to participate in this study. The detail description of the measurements protocol is presented in appendix B.

3.1.4. Skin preparation for cream measurements. In order to test the effect of active or inactivate sweat glands on the reflection coefficient, a cream containing a snake venom-like synthetic tripeptide was applied to the test area of the palm. The tripeptide acted as an antagonist of the postsynaptic muscular nicotinic acetylcholine membrane's receptor (mnAChR), situated on the nerve synapse controlling the eccrine sweat gland (McArdle *et al* 1999). The measurements of the reflection coefficient were repeated in calm and excited states of the subjects. The active lifetime of the tripeptide action is a few hours. The same subjects were then treated on the following day with a placebo cream, based on the same matrix but not containing the synthetic tripeptide (Ziegler and Heidl 2007). This was done in order to account for any hydrating effects of the cream itself.

3.1.5. Cuff pressure measurements. The control of blood perfusion in the skin layer was performed by a cuff pressure device. The cuff pressure was increased (0–100 mmHg) to the desired level and held steady for 3 min before the measurement. Each measurement was repeated three times. After the maximum pressure was achieved (100 mmHg), the pressure was reduced and measurements were made using the same routine.

4. Results and discussion

4.1. NF measurements—comparison with the theoretical model

For NF measurements, the complex reflection coefficient of the palm was calculated using equations (A.4)–(A.6) (Appendix A). A typical series of measurements for one subject is presented in figure 11.

As can be seen in figure 11, there is a pronounced difference between the reflectance spectra that were measured in the calm state and immediately after a period of physical activity. In the subsequent measurements, as the subject relaxed back to the calm state, the spectral response of the coefficient also relaxed back toward its initial curve. These observations are in good agreement with the results of the simulation and demonstrating a clear dependence of the level of the reflection coefficient at the minimum point on the conductivity of the coils that is linked to the level of relaxation following intense physical activity (see figure 8).

In order to compare the changes in the reflectance as a function of time to simultaneous variations of the measured physiological parameters (pulse rate, blood pressure and skin

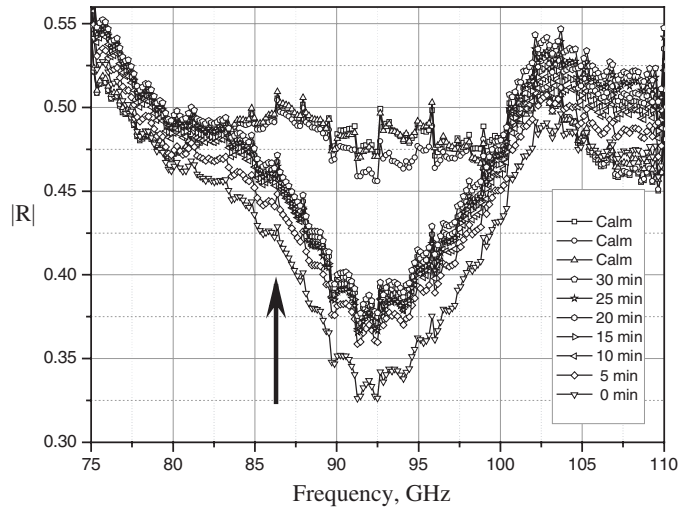


Figure 11. Measurements of the modulus of the reflection coefficient R of the human palm provided for the frequency region 75–110 GHz (see equation (A.7)). Measurements were done using VNA HP 8510C in the near field in a calm state and then during 30 min relaxation after intense physical activity. The arrow on the graph indicates the direction of the time line and shows how the signal returns to the calm state with a relaxation (Feldman *et al* 2008). The subject was an Asian male aged 33. (Reproduced with permission from Feldman *et al* (2008); Copyright 2008, American Physical Society.)

temperature) of the subjects, we calculated the integral signal power $\langle I(t) \rangle$ obtained from the reflection coefficient measurements in the frequency band 75–110 GHz:

$$\langle I(t) \rangle = \frac{1}{(f_2 - f_1)} \int_{f_1}^{f_2} |R(f, t)|^2 df, \quad (7)$$

where $R(f, t)$ is the palm reflection coefficient measured from the subject following physical activity, $f_1 = 75$ GHz and $f_2 = 110$ GHz.

In figure 12, the value $W(t) = \langle I \rangle_{\max} - \langle I(t) \rangle$ is presented together with concurrent measurements of the skin temperature and the pulse rate. The first measurement (at $t = 0$) was taken for a subject at rest following 20 min of intense exercise. Thirty similar measurements were repeated at 1 min intervals. It can be seen that the integral signal ($W(t)$) is not correlated with the skin temperature of the subject, whereas it is highly correlated with the pulse rate.

4.2. 'Distance measurement' measurements

The second set of measurements was done in a system that was configured for distance measurements. As described in detail above, the right palm of the subject was held steady by a stand that was placed 22 cm from the horn antenna at the input of the VNA, and a dielectric lens was used to collimate the beam as it is shown in detail in figure 10. Similar sets of measurements were taken from 13 subjects differing in gender, age and ethnic origin. Each set included a measurement of the skin reflectance, and concurrent recordings of the pulse rate, the systolic blood pressure and the skin temperature (Feldman *et al* 2008). The subjects performed 20 min of jogging after which a sequence of 30 sets of measurements were taken at

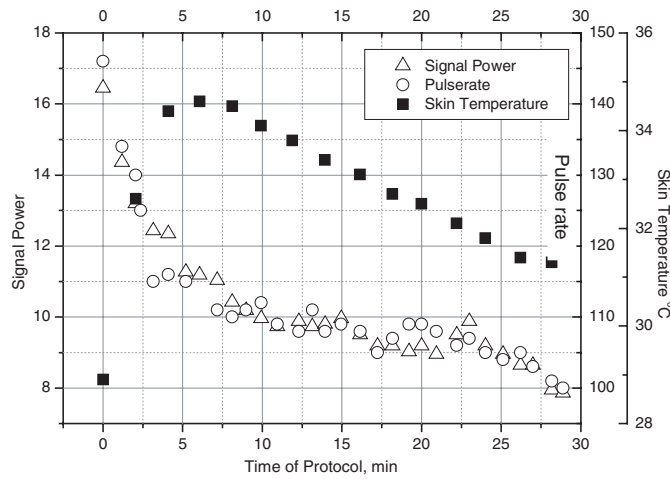


Figure 12. The typical time behaviours of the signal power obtained from the reflection coefficient of the subject’s palm, a concurrent pulse of the same person at rest following intense exercise and the temperature of the subject’s skin. The subject is a Caucasian male aged 35.

1 min intervals according to the protocol (see Appendix B). The skin reflectance is presented in terms of its frequency-averaged relative signal intensity given by

$$\langle W_{rel}(t) \rangle_f = \frac{1}{(f_2 - f_1)} \int_{f_1}^{f_2} \left| \frac{U_{subject}(f, t)}{U_{reference}(f, t)} \right|^2 df, \quad (8)$$

where $U_{subject}(f)$ is the reflected signal from the subject after physical activity, $U_{reference}(f)$ is the reflected signal measured from the subject while sitting at rest before engaging in physical activity and the frequency range was between $f_1 = 75$ GHz and $f_2 = 110$ GHz.

It can be seen that after the physical activity, an exponential-like relaxation is observed in the signal intensity, which is correlated with the relaxation of the subject’s pulse rate and the systolic blood pressure (figure 13) (Feldman *et al* 2008). The results for the entire ensemble of 13 subjects are summarized in figure 14, in which the normalized ensemble average of $\langle W_{rel} \rangle$ (‘Normalized Signal’ in the figure) for the 30 measurement points is presented against the respective ensemble average of the systolic blood pressure. A strong correlation between the reflection average and the respective blood pressure average is clearly observed. The correlation was quantified in terms of the correlation parameter given by

$$r = \frac{\sum_{i=1}^n (x_i - \bar{x})(y_i - \bar{y})}{\sqrt{\sum_{i=1}^n (x_i - \bar{x})^2} \sqrt{\sum_{i=1}^n (y_i - \bar{y})^2}}, \quad 0 \leq r \leq 1. \quad (9)$$

The value of r for the correlation between the reflection signal and the blood pressure was found to be $r = 0.984$, very close to unity. This indeed indicates the strong correlation between them and expresses the fact that essentially they exhibit similar temporal behaviour. The correlation of $\langle W_{rel} \rangle$ with the pulse rate yielded $r = 0.85$ (see figure 15).

In order to substantiate that the observed phenomena are indeed governed by the morphology of the sweat duct, it is necessary to rule out other mechanisms that might affect the measurement. In biological systems, at this frequency range, the only potential mechanisms originate from the absorption spectrum of water. As the main absorption peak of water is at 18 GHz, it is possible that a significant tail in the lower end of the frequency

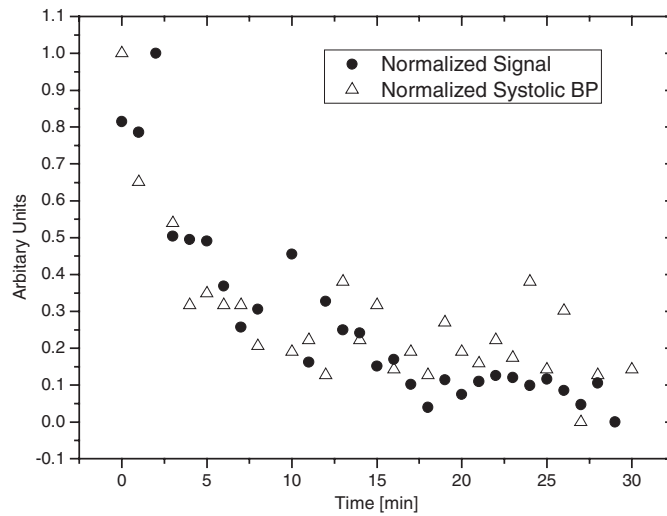


Figure 13. The frequency-averaged normalized signal intensity $\langle W_{\text{rel}}(t) \rangle_f$ recorded from reflection coefficient measurements in the frequency band 75–110 GHz of the palm of a subject at rest following 20 min of intense physical activity (Feldman *et al* 2008). To avoid reflection from surface water, the hand was kept dry. Concurrently, the normalized systolic blood pressure, measured for the subject during the experiment, is plotted. Similar temporal behaviour is noted. The subject was a Caucasian male aged 34.

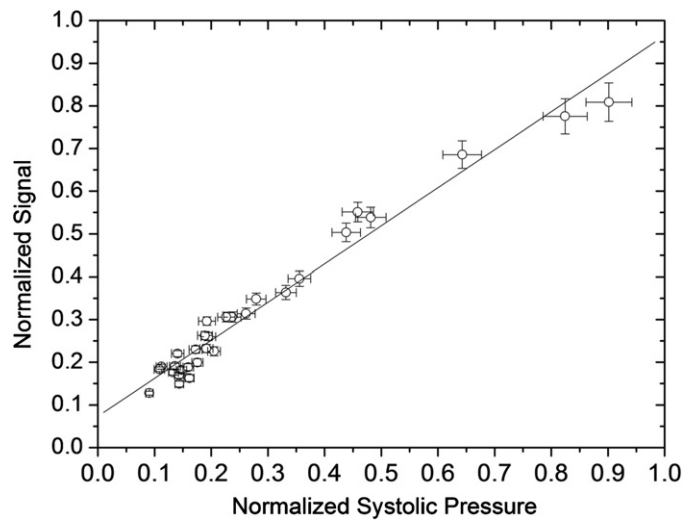


Figure 14. The correlation graph between the systolic blood pressure and $\langle W_{\text{rel}}(t) \rangle_f$, obtained from the average of 13 subjects measured as they relaxed for a period of 30 min after intensive physical activity (Feldman *et al* 2008). (Reproduced with permission from Feldman *et al* (2008); Copyright 2008, American Physical Society.)

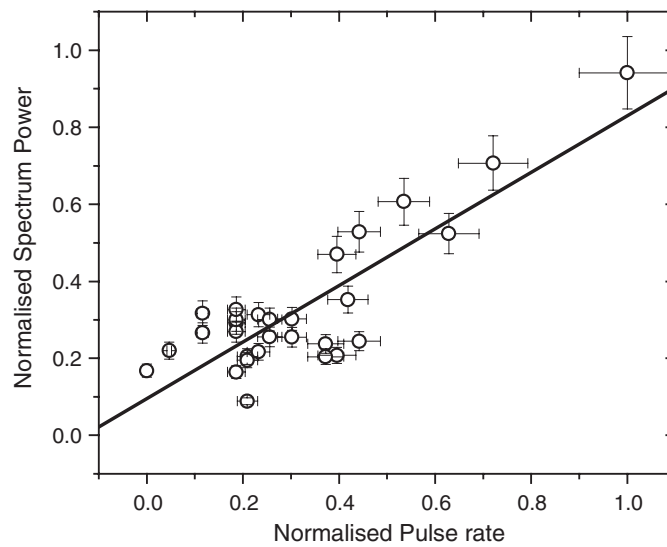


Figure 15. The correlation graph between pulse rate and $\langle W_{\text{rel}}(t) \rangle_f$, obtained from the average of 13 subjects measured as they relaxed for a period of 30 min after intensive physical activity.

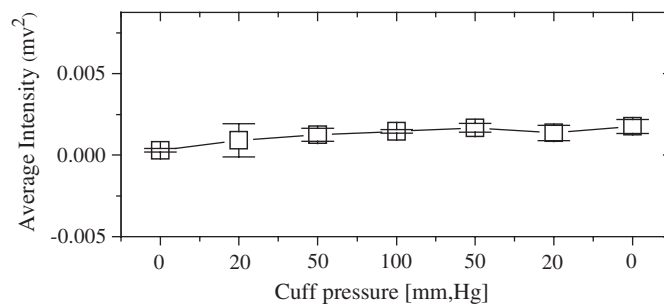


Figure 16. The signal intensity versus the cuff pressure.

range measured (Kaatze 1995) will be apparent in the presented results. Thus, it is *a priori* possible that the observed phenomena reflect changes that occur in the water content in the skin organ and underlying tissue, e.g. due to capillary blood flow/perfusion characteristics resulting from the physical activity. In order to eliminate this possibility, an additional set of measurements using a pressure cuff was performed. This enabled the control of blood perfusion during the measurement without activating the sweat gland system. The reflection coefficient was measured from the palm while the subject was seated at rest. The results of this set of measurements are shown in figure 16, which represents the averaged signal intensity obtained for each cuff pressure level. It was expected that the increasing pressure applied by the cuff would reduce the capillary blood flow (Murray and Marjanovic 1997) and result in an increase of the total amount of blood in the skin and underlying tissue (Douven and Lucassen 2000). Measurements at different pressures show no noticeable dependence of the reflectance signal on the capillary blood flow/perfusion change in volume fraction in this tissue compartment.

The results of the measurements involving the tripeptide application are illustrated in figure 17. It can be seen that when the active component was used, the signal intensity is

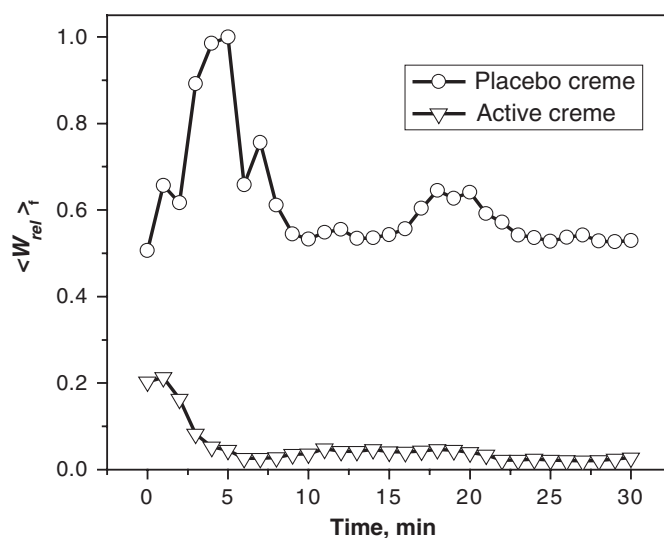


Figure 17. The sweat ducts on the palm were temporally deactivated by applying a cream containing a synthetic tripeptide, 120 min before measurement. As a control, the experiment was repeated using only the crème without the active compound. The relative signal intensity received from the treated hand shows the lowered amplitude compared to that of the hand treated with a placebo. The amplitudes are normalized by the maximum amplitude recorded when using a placebo crème (Feldman *et al* 2008).

lowered significantly. This clearly indicates the important role of the level activity of the sweat glands in the received signal (Feldman *et al* 2008).

In summary, the results presented herein indeed indicate that the reflectance of the skin in the EHF range is correlated with the state of activity of the perspiration system. As pointed out above, this was predicted by observing that the tips of the ducts of the eccrine sweat glands have a coil-like structure. The ducts emerge from the glands that are embedded at the bottom of the dermis and pass through the dermis and epidermis to the pore at the external layer of the skin—the stratum corneum. More specifically, the coil-like tips of the ducts are embedded in the hydrophobic epidermis, the dielectric constant of which is lower than that of the hydrophilic dermis. Thus, the dermis and epidermis in which the ducts are embedded can be regarded as a multilayered dielectric composite.

This brought forward the supposition that as electromagnetic entities, the tips of the sweat glands are expected to have the characteristics of low Q helical antennas. Taking into account the typical dimension of the ducts and the dielectric constants of their surrounding tissues indicate that the dielectric response of the ducts is expected to be pronounced mostly in the EHF range, namely in the sub-THz region.

It is implicitly assumed in this prediction that the ducts are electrically conductive at the EHF range. A potential mechanism that can support conductivity at this frequency range is proton hopping.

It is known that the human skin contains approximately 2–5 million eccrine sweat glands distributed over most of the body with higher density in several areas such as the palms, the forehead and the soles (Nishiyama *et al* 2001, Salvesen 2001). Each eccrine gland is connected to the skin surface by a helical sweat duct; hence, the skin organ is in fact an array of helical antennas that operate in the EHF range. Thus, the skin organ in its entirety can be

regarded as a 'bio-metamaterial' with an electromagnetic response in the range of sub-THz frequencies that is governed by the morphology of the structure, namely the coil-like structure of the ducts' tips.

5. Conclusions

It was shown that the reflectance spectrum depends strongly on the state of the perspiration system. The prime function of the perspiration system is heat regulation. However, it is well established that the level of activity of the perspiration system manifests both the physiological condition and the mental state. Hence, other parameters that reflect the conditions that activate the perspiration system are also expected to be correlated with the EM response. It was shown that during the relaxation period that followed physical activity, the temporal change in physiological markers (systolic blood pressure and heart beat rate) were strongly correlated with the reflectance signal. It is well known that the perspiration system is also responsive to emotional and gustatory excitations (Landis and Keefe 1983, Folk and Semken 1991, Kamei *et al* 1998). Moreover, it was shown that the spatial distribution of its activity is the characteristic of the mechanism that initiated the system. Thus, it is reasonable to assume that this should also be manifested in the spatial distribution of the reflectance spectrum of the skin in the range of sub-THz frequencies. Hence, mapping the reflectance signal can provide more detailed information about the state of the subject under examination. This possibility should be explored in detail.

Finally, the results described above were produced by sampling the reflectance long after the excitation that caused the changes in the reflectance to happen. It is yet to be determined, what is the temporal response of the reflectance signal to both physical and emotional excitations. The combination of the reflectance spatial and temporal response has the potential to lead to the creation of a generic method for remote sensing of the physical and emotional state of human beings.

Acknowledgments

We thank Professor B Kapilevich at Ariel College for helpful discussions, Professor D Davidov and Dr M Golosovsky of the Racah Institute of Physics of the Hebrew University of Jerusalem for their kind assistance, and Dr A Greenbaum, Mrs Osnat Heller and other members of the Dielectric Spectroscopy Laboratory at Department of Applied Physics HUJI for comprehensive help in the VNA measurements. This work was supported by THE FIRST Program of the ISRAEL SCIENCE FOUNDATION (grant no 1128/05), the Israeli Ministry of Science, Culture and Sport (grant no 3/4602) and the Yeshaya Horowitz Association.

Appendix A. The vector network analyser (VNA) measurements and data treatment in the near field measurements

In near field VNA measurements (see figure 9), propagation and multiply reflections can be considered in terms of the principal waveguide mode (TE_{10}). The calibration routine was based on two reference measurements of the signal: (i) in a standard reference configuration whereby a measurement of the reflection from the Teflon/air boundary was made; and (ii) in a total reflection configuration whereby the horn antenna covered by the Teflon plate terminated by a metallic plate. These reference measurements represent the highest range of signal amplitudes that could be achieved in the NF measurement setup.

In the OO' plane of the waveguide (figure 9), the complex reflected signal can be written as

$$U(\omega) = V_0 \exp(i2kl_1) \cdot [R_{11} + W_{12}W_{21}R_{TP}(\omega) \cdot \exp(i2kl\sqrt{\varepsilon})]. \quad (\text{A.1})$$

Here, $k = \omega/c$ is the wave number in free space ($\omega = 2\pi f$), f (Hz) is the frequency, c is the velocity of light, V_0 is the amplitude of the input signal, l_1 is the distance from the section OO' to the Teflon plate, $\varepsilon \cong 2$ is the dielectric permittivity of Teflon, $R_{11} = (1 - \sqrt{\varepsilon})/(1 + \sqrt{\varepsilon})$ is the reflection coefficient from the air/Teflon boundary, $R_{22} = -R_{11}$ is the reflection coefficient from the Teflon/air boundary, $W_{21} = 1 + R_{11}$ is the transition coefficient through the Teflon/air interface, $W_{12} = 1 + R_{22}$ is the transition coefficient through the air/Teflon interface and $R_{TP}(\omega)$ is the unknown complex reflection coefficient from the Teflon/palm boundary.

Due to the small reflection coefficient at the Teflon/air interface, $|R_{11}| = |R_{22}| \cong 0.17 \ll 1$, only the first two terms in the expansion of the multiple reflection series are taken into account in equation (A.1).

As pointed out above, two reference measurements were done prior to the measurements of the palm reflection signal: a ‘Teflon plate’ measurement and a ‘total reflection’ measurement. The total reflection measurement was done with a metal plate attached to a Teflon plate. This reference signal can be represented similarly to (A.1):

$$U_M(\omega) = V_0 \exp(i2kl_1) \cdot [R_{11} + W_{12}W_{21}R_M \cdot \exp(i2kl\sqrt{\varepsilon})], \quad (\text{A.2})$$

where $R_M = -1$ is the reflection coefficient from the Teflon/metal interface. For the ‘open end’ reference measurement, the Teflon plate was left exposed to free space so that

$$U_T(\omega) = V_0 \exp(i2kl_1) \cdot [R_{11} + W_{12}W_{21}R_{22} \cdot \exp(i2kl\sqrt{\varepsilon})]. \quad (\text{A.3})$$

Using relationships (A.1)–(A.3) and the differential linear-fractional technique, the Teflon/palm reflection coefficient $R_{TP}(\omega)$ can be evaluated by computing $Q(\omega)$ given by

$$Q(\omega) = \frac{U(\omega) - U_T(\omega)}{U(\omega) - U_M(\omega)} = \frac{R_{11} + R_{TP}(\omega)}{1 + R_{TP}(\omega)}. \quad (\text{A.4})$$

In terms of $Q(\omega)$, the complex Teflon/palm reflection coefficient is given by

$$R_{TP}(\omega) = \frac{Q(\omega) - R_{11}}{1 - Q(\omega)}. \quad (\text{A.5})$$

Finally, in terms of $R_{TP}(\omega)$, the complex air/palm reflection coefficient $R(\omega)$ is given by

$$R(\omega) = \frac{R_{11} + R_{TP}(\omega)}{1 + R_{11} \cdot R_{TP}(\omega)}. \quad (\text{A.6})$$

Note, that the obtained air/palm reflection coefficient $R(\omega)$ is the general reflection coefficient for monochromatic plane waves. The modulus of $R(\omega)$ is related to the spectral intensity $I(\omega)$ of the reflected waves by

$$|R(\omega)| = \sqrt{I(\omega)}. \quad (\text{A.7})$$

Appendix B. The measurement protocol

The schematic representation of the measurement protocol is shown in figure B1. Initially the system was focused, calibrated and stabilized. The signal power was set to 1 dBm. In the case of DM, the same calibration standards were used again.

However, the point of reference was moved to the stand/palm interface.

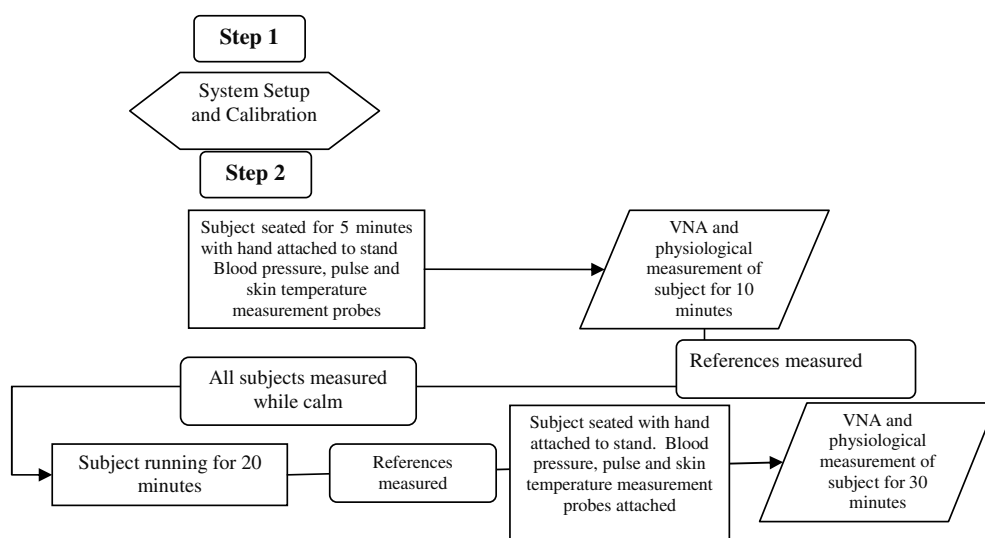


Figure B1. Schematic representation of the measurement protocol. The arrow represents the time direction.

For a period of 6 h prior to the measurement, the subjects did not take stimulants such as caffeine or sugars. Initially, each subject sat at rest for 5 min with the right hand attached to the stand, skin temperature measurement probes attached and the left arm connected to a blood pressure monitor. During this time, the subject became accustomed to the measurement conditions. Then, in this ‘calm’ state, the subject reflection coefficient, systolic/diastolic blood pressure, pulse and skin temperature were measured for 10 min at 1 min intervals. The reflectance was measured in the frequency range 75–110 GHz. After the measurements of all the subjects in the relaxed state were completed, each subject performed 20 min of intense jogging followed by a sequence of 30 sets of ‘excited state’ measurements, conducted by the same protocol as before. To avoid reflection from the sweat accumulated on the surface of the skin, the palm was wiped dry before every measurement. Additionally, the references were measured before and after the measurement set of each subject in the calm and excited states.

References

- Balanis A A C 2005 *Antenna Theory: Analysis and Design* (NJ: Wiley) chapter 10
- Caspers P J, Wucassen L G, Bruining H A and Puppels G J 2000 Automated depth-scanning confocal Raman microspectrometer for rapid *in vivo* determination of water concentration profiles in human skin *J. Raman Spectrosc.* **31** 813–8
- Covington A K, Bates R G and Durst R A 1985 Definition of pH scales, standard reference values, measurement of pH and related terminology *Pure Appl. Chem.* **57** 531–42
- Cukierman S 2000 Proton motilities in water *Biophys. J.* **78** 1825–34
- Douven L F A and Lucassen G W 2000 Retrieval of optical properties of skin from measurement and modeling the diffuse reflectance *Proc. SPIE* **3914** 312–23
- Ellison W J, Lamkaouchi K and Moreau J M 1996 Water: a dielectric reference *J. Mol. Liq.* **68** 171–279
- Feldman Y, Puzenko A, Ben Ishai P, Caduff A and Agranat A J 2008 Human skin as arrays of helical antennas in the millimeter and submillimeter wave range *Phys. Rev. Lett.* **100** 128102
- Folk G E and Semken H A 1991 The evolution of sweat glands *Int. J. Biometeorol.* **35** 180–6

- Gabriel S, Lau R W and Gabriel C 1996 The dielectric properties of biological tissues: II. Measurements in the frequency range 10 Hz to 20 GHz *Phys. Med. Biol.* **41** 2251–69
- Goldsmith L A 1999 *Fitzpatrick's Dermatology in Internal Medicine* vol 1 ed I M Freedberg, A Z Eisen and K Wolff (New York: McGraw-Hill) pp 155–63
- Graham-Brown R and Burns T *et al* 2002 *Lecture Notes on Dermatology* (Oxford: Blackwell) pp 1–8
- Grimmes S and Martinsen Ø G 2000 *Bioimpedance and Bioelectricity Basics* (London: Academic)
- Guyton A C 1991 *Textbook of Medical Physiology* 8th edn (Philadelphia, PA: Saunders) pp 800–7
<http://www.mydr.com.au/default.asp?Article=3718>
- Inoue Y, Shibasaki M, Hirata K and Araki T 1998 Relationship between skin blood flow and sweating rate, and age related regional differences *Eur. J. Appl. Physiol.* **79** 17–23
- Jacubovic H R and Ackerman A B 1992 *Dermatology* vol 1 ed S L Moschella and H J Hurley (Philadelphia, PA: Saunders) pp 66–77
- Kaatze U 1989 Complex permittivity of water as a function of frequency and temperature *J. Chem. Eng.* **34** 371–4
- Kaatze U 1995 Fundamentals of microwaves *Radiat. Phys. Chem.* **45** 539–48
- Kamei T, Tsuda T, Kitagawa S, Naitoh K, Nakashima K and Ohhashi T 1998 Physical stimuli and emotional stress-induced sweat secretions in the human palm and forehead *Anal. Chim. Acta* **365** 319–26
- Knüttel A and Böchlau-Godau M 2000 Spatially confined and temporally resolved refractive index and scattering evaluation in human skin performed with optical coherence tomography *J. Biomed. Opt.* **5** 83–92
- Knüttel A, Bonev S and Knaak W 2004 New method for the evaluation of *in vivo* scattering and refractive index properties obtained with optical coherence tomography *J. Biomed. Opt.* **9** 265–73
- Krasnolovets V V, Tomchuk P M and Lukyanets S P 2003 Proton transfer and coherent phenomena in molecular structures with hydrogen bonds *Adv. Chem. Phys.* **125** 351–548
- Kraus J D 1950 *Antennas* (New York: McGraw-Hill) pp 382–90
- Landis S C and Keefe D 1983 Evidence for neurotransmitter plasticity *in vivo*—developmental changes in properties of cholinergic sympathetic neurons *Dev. Biol.* **98** 349–72
- McArdle J J, Lentz T L, Witzemann V, Schwarz H, Weinstein S A and Schmidt J J 1999 Waglerin-1 selectively blocks the epsilon form of the muscle nicotinic acetylcholine receptor *J. Pharmacol. Exp. Ther.* **289** 543–50
- Murray A and Marjanovic D 1997 Optical assessment of recovery of tissue blood supply after removal of externally applied pressure *Med. Biol. Eng. Comput.* **35** 425–7
- Neerken S, Lucassen G W, Bisschop M A, Lenderink E and Nuijs T A M 2004 Characterization of age-related effects in human skin: a comparative study that applies confocal laser scanning microscopy and optical coherence tomography *J. Biomed. Opt.* **9** 274–81
- Nishiyama T, Sugenoja J, Matsumoto T, Iwase S and Mano T 2001 Irregular activation of individual sweat glands in human sole observed by a videomicroscopy *Auton. Neurosci.-Basic Clin.* **88** 117–26
- Nouveau-Richard S, Monot M, Bastien P and de-Lacharrière O 2004 *In vivo* epidermal thickness measurement: ultrasound vs. confocal imaging *Skin Res. Technol.* **10** 136–40
- Ogawa T and Sugenoja J 1993 Pulsatile sweating and sympathetic sudomotor activity *Japan. J. Physiol.* **43** 275–89
- Perini R, Orizio C, Comande A, Castellano M, Beschi M and Veicsteinas A 1989 Plasma norepinephrine and heart rate dynamics during recovery from submaximal exercise in man *Eur. J. Appl. Physiol.* **58** 879–83
- Peters M J, Stinstra J G and Hendriks M 2001 Estimation of the electrical conductivity of human tissue *Electromagnetics* **21** 545–57
- Pethig R 1987 Dielectric properties of body tissues *Clin. Phys. Physiol. Meas.* **8** 5–12
- Pethig R 1979 *Dielectric and Electronic Properties of Biological Materials* (New York: Wiley)
- Peyman A, Gabriel C and Grant E H 2007 Complex permittivity of sodium chloride solutions at microwave frequencies *Bioelectromagnetics* **28** 264–74
- Pozar D 1998 *Microwave Engineering* 2nd edn (New York: Wiley) pp 196–201
- Sadeghi R R and Cheng H P 1999 The dynamics of proton transfer in a water chain *J. Chem. Phys.* **111** 2086–94
- Salvesen R 2001 Innervation of sweat glands in the forehead. A study in patients with Horner's syndrome *J. Neurol. Sci.* **183** 39–42
- Sandby-Møller J, Poulsen T and Wulf H C 2003 Epidermal thickness at different body sites: relationship to age, gender, pigmentation, blood content, skin type and smoking habits *Acta Derm. Venereol.* **83** 410–3
- Shamsuddin A K M and Togawa T 1998 Continuous monitoring of sweating by electrical conductivity measurement *Physiol. Meas.* **19** 375–82
- Shamsuddin A K M and Togawa T 2000 Continuous monitoring of single sweat gland activity *Physiol. Meas.* **21** 535–40
- Smith S R and Foster K R 1985 Dielectric properties of low-water-content tissues *Phys. Med. Biol.* **30** 965–73
- Takagi S and Tagawa M 1957 Predominance of right-handed spirals in the intraepidermal sweat ducts in man and the primates *Japan. J. Physiol.* **7** 113–8

- Takashima S 1989 *Electrical Properties of Biopolymers and Membranes* (Bristol: Institute of Physics Publishing)
- Waller J M and Maibach H I 2005 Age and skin structure and function, a quantitative approach (I): blood flow, pH, thickness, and ultrasound echogenicity *Skin Res. Technol.* **11** 221–35
- Wang Z, Deurenberg P, Wang W, Apietrobelli A, Baumgartner R N, Steven B and Heymsfield S B 1999 Hydration of fat-free body mass: review and critique of a classic body-composition constant *Am. J. Clin. Nutr.* **69** 833–41
- Ziegler H and Heidl M 2007 Biomimetic tripeptides for improved dermal transport *Cosmet. Toiletries* **122** 59–67